Capillarity Guided Patterning of Microliquids

Myeongwoo Kang, Woohyun Park, Sangcheol Na, Sang-Min Paik, Hyunjae Lee, Jae Woo Park, Ho-Young Kim, and Noo Li Jeon**

***S**oft lithography and other techniques have been developed to investigate biological and chemical phenomena as an alternative to photolithography-based patterning methods that have compatibility problems. Here, a simple approach for nonlithographic patterning of liquids and gels inside microchannels is described. Using a design that incorporates strategically placed microstructures inside the channel, microliquids or gels can be spontaneously trapped and patterned when the channel is drained. The ability to form microscale patterns inside microfluidic channels using simple fluid drain motion offers many advantages. This method is geometrically analyzed based on hydrodynamics and verified with simulation and experiments. Various materials (i.e., water, hydrogels, and other liquids) are successfully patterned with complex shapes that are isolated from each other. Multiple cell types are patterned within the gels. Capillarity guided patterning (CGP) is fast, simple, and robust. It is not limited by pattern shape, size, cell type, and material. In a simple three-step process, a 3D cancer model that mimics cell–cell and cell–extracellular matrix interactions is engineered. The simplicity and robustness of the CGP will be attractive for developing novel in vitro models of organ-on-a-chip and other biological experimental platforms amenable to long-term observation of dynamic events using advanced imaging and analytical techniques.*

1. Introduction

Despite the short history, nonconventional microscale patterning techniques such as soft lithography have matured considerably in recent years.[1,2] Micropatterning techniques offer many advantages over conventional large scale methods based on photolithography and in biological research. Conventional research tools have severe limitations in terms of compatibility in handling live cells. Alternatives such soft lithography and others have been developed to fill this gap of single cell patterening/manipulation,[3–8] production of complex chemical gradients,[9] patterning for coculture tissue engineering,[10–14] and others. Nonconventional, "soft" micropatterning techniques have gained considerable appeal for biological and chemical research.[11,13,15–18]

One of the widely adopted method for cell patterning is based on soft lithography techniques such as microcontact printing (μCP)[19] and micromolding in capillaries (MIMIC).[1,15] Microcontact printing and MIMIC transfer protein or extracellular matrix (ECM) patterns on a substrate which is used for selective cell attachment.[20] Although these methods can make small and precise patterns, they can be only applied to the adherent cells and require additional processes such as metal deposition and etching or oxidation.[21] Furthermore, μCP and MIMIC can produce limited

M. Kang, W. Park, S. Na, H. Lee, J. W. Park, Prof. N. L. Jeon
Division of WCU (World Class University)
Multiscale Mechanical Design
Seoul National University
Seoul, Korea
E-mail: njeon@snu.ac.kr
S.-M. Paik
Interdisciplinary Program for Bioengineering
Seoul National University
Seoul, Korea
Prof. H.-Y. Kim, Prof. N. L. Jeon
Department of Mechanical and Aerospace Engineering
Seoul National University
Seoul, Korea
E-mail: hyk@snu.ac.kr

DOI: 10.1002/smll.201403596

patterns such as lines or spots and it is difficult to produce functional multicellular patterns or cocultures with three or more cell types.[22]

Recently, many efforts have been devoted to pattern cells on 2D surfaces or in 3D gels to mimic in vivo microenvironment. Cells were patterned within hydrogels (i.e., collagen or others),[23,24] UV curable materials (i.e., poly(ethylene glycol) diacrylate (PEG-DA)),[11,25,26] and droplets.[27,28] Another approach to fix the cell position is using external forces to move cells to specific positions by optical tweezers, digitalized Braille pins,[29,30] microtraps using hydrodynamics,[16,31–34] and dielectrophoresis.[9] These techniques provide more advanced patterning capability and cell compatibility.

In this study, we introduce a new method for rapid patterning by simple aspiration of microfluidic device. Based on understanding of the hydrodynamics, we have designed structures to control the shape of menisci and their dynamics to generate complex microliquid patterns of variable size and shapes (simulation and experimental results show excellent agreement). Using this new technique called capillarity-guided patterning (CGP), we demonstrated variety of patterns of cells trapped in hydrogel (i.e., cell array, neural network and blood vessel network and cancer-human umbilical vein endothelial cells (HUVEC) coculture). Furthermore, we could produce complex patterns consisting of multiple materials (or materials with different composition). Compared to other patterning methods, CGP is (i) extremely simple and fast, (ii) robust and reliable, (iii) flexible in terms of possible pattern shape, size, and material, (iv) no need for special equipment or complex processes, and (v) scalable to large area patterning.

We expect CGP to become a new method of microscale patterning based on fluid mechanics principles. CGP provide simplicity and robustness and it will be attractive in developing novel biological experimental platforms such as organ-on-a-chip and high throughput screening system.

2. Results

2.1. Engineering Meniscus Dynamics with Microstructures

We first describe the dynamics of liquid meniscus that advances and snaps as the volume of liquid decreases in the microchannel. **Figure 1**A shows the schematic of the experimental setup for observing meniscus dynamics when liquid filled channel is drained. The device design incorporates a number of posts strategically positioned within the main microchannel. When a liquid-filled microchannel is drained, liquid–air interface contacting the posts forms a number of menisci along the channel width. When the meniscus touches the posts, the interface straddling the posts advances first while the contact line on the post surface moves around it. Thus, the meniscus bulges into the liquid region. The shape of meniscus is influenced by the property of liquid–solid interaction (surface tension) and pressure difference between liquid and air. The curvature of the meniscus is determined by the Young–Laplace equation, which describes the pressure difference across the interface, Δp, a product of the liquid–gas surface tension γ and interface curvature κ: $\Delta p = \gamma\kappa$. The curvature of interface is given by $\kappa = 1/R_1 + 1/R_2$ (see Figure 1B), where R_2 can be assumed constant. The radius of curvature from a top view, R_1, must be identical for each section of the meniscus comparted by the posts because the pressure difference, Δp, should be uniform. Hence, the larger the gap between the posts, the meniscus advances further into the liquid region, increasing the dry region.

We now consider the bulging process of the meniscus in detail. Figure 1B illustrates the shape evolution of the meniscus as the contact line moves along the circular post surface in the direction of increasing α (angle between the center of post and the contact point of meniscus at the largest gap). A geometric consideration readily relates R to α as $\mathrm{R} = (L_1 - 2r\sin\alpha)/2\sin\alpha$, where L_1 is the largest gap between the posts and r is the radius of the post. Here the receding contact angle is taken to be zero due to the wettability of the post surface. For $0 \le a \le \pi/2$, R decreases until it reaches $R_m = (L_1 - 2r)/2$ when $\alpha = \pi/2$. R increases afterwards, i.e., for $\alpha > \pi/2$. The meniscus between the posts of narrower gaps, L_2 ($L_2 < L_1$), also has the radius of curvature R when viewed from the top. This allows us to predict the location of the contact line on the posts, β in Figure 1B, $\beta = \sin^{-1}\left(L_2/2(R+r)\right) = \sin^{-1}\left(L_2\sin\alpha/L_1\right)$. β increases as α grows from 0 to $\pi/2$ but rather decreases with $\alpha > \pi/2$. Consequently, β cannot exceed $\pi/2$, implying that the meniscus between the posts of narrower gaps is always pinned in the region $\beta < \pi/2$.

Figure 1C shows the plot of the radius of curvature and the corresponding distance between the pole and the starting line, D (Figure 1B), for a meniscus between the post of the largest gap as a function of α. We can simply get $D = R + r - L_1/(2\tan\alpha)$. Despite nonmonotonic behavior of R with α, D increases monotonically for entire range of α. On the contrary, the advanced distance at the narrower gap, d, can be expressed as $d = R + r - L_2/(2\tan\beta)$. As the expression of d, the meniscus at narrower gap advances until $\alpha < \pi/2$ and retreats after $\alpha > \pi/2$ because β increases until $\alpha < \pi/2$ and decreases after $\alpha > \pi/2$. Figure 1D shows the advanced distances at various gaps (D and d).

As the geometrical analysis indicates, the meniscus dynamics can be separated into two phases. In the first phase, all menisci bulge into liquid region until $\alpha < \pi/2$ but after the transition ($\alpha = \pi/2$), only the meniscus at the largest gap advances while all other menisci retreat to maintain constant radius of curvature dictated by constant Δp.

To confirm and compare the mathematical model for the shape of menisci of different gap distances, we performed experiments with gap distances from 100 to 400 μm between posts. Figure 1E,F shows the simulation and experimental results, respectively, which reveal favorable agreement between theory and experiment. All menisci in the channel advance and grow during initial phase 1, shown in the first two pictures in Figure 1E,F. When the radii are minimized at the transition point to phase 2 ($\alpha = \pi/2$), only the meniscus at the largest gap (400 μm) bulges while the other menisci retreat.

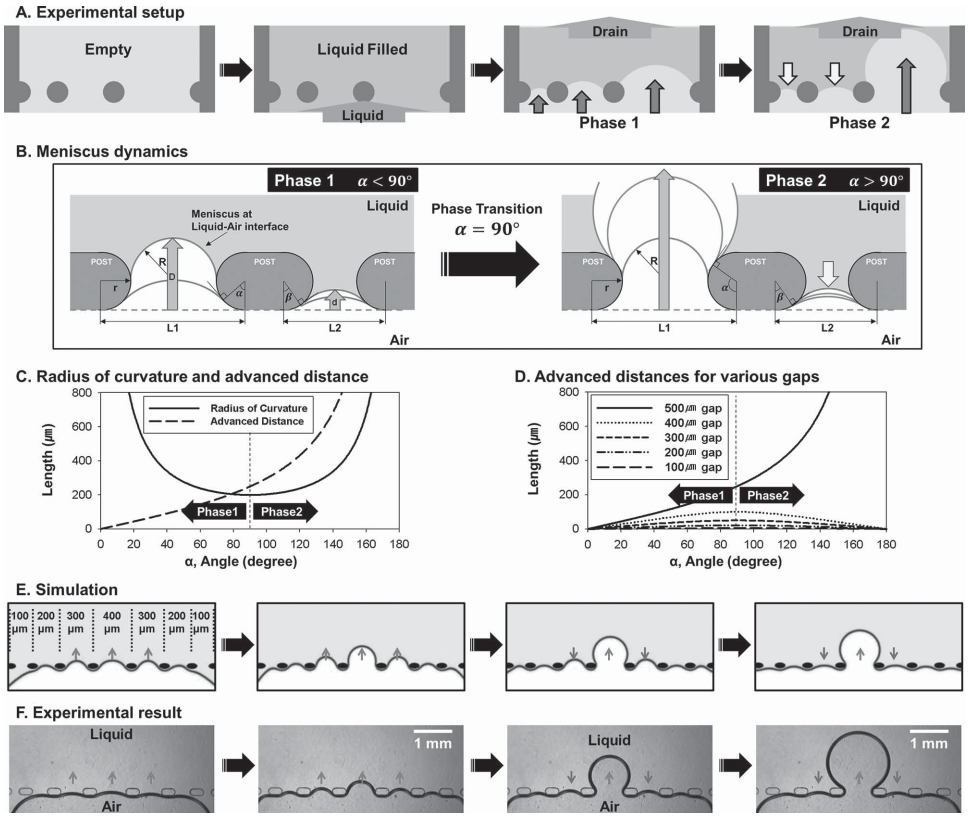

Figure 1. Engineering meniscus dynamics with microstructures. Experimental setup and schematic of meniscus dynamics during draining of liquid filled microchannel. A) Simplified schematic of microchannel containing isolated microstructures with various gap distances. Menisci shape and extent of advancement are dependent on gap distance when the liquid filled channel is drained. Menisci move in the direction of fluid drainage. The menisci shape and extent of advancement are dependent on gap distance. At certain point, only the meniscus at the largest gap advance and the rest retreat. B) Geometric analysis of meniscus dynamics starting from baseline (dotted line). The meniscus dynamics undergoes a transition when $\alpha = \pi/2$, (α is the angle between the center of post and the contact point of meniscus at the widest gap. In phase 1, all menisci advance toward direction of liquid drainage and the while the radii of curvature decrease. In phase 2, the meniscus at widest gap advances but all other menisci retreat toward air region while the radii of curvature increase. C) Plot of radius of curvature and meniscus advancement based on geometric analysis at the widest gap according to the angle α. The radius of curvature decreases from infinite to $(L_1 - 2r)/2$ while the angle α increases from 0 to $\pi/2$. After the transition at $\alpha = \pi/2$, the radius of curvature increases when $\alpha > \pi/2$. The advanced distance D at the widest gap increases while the angle α increases from 0° to 180°. D) Plot of advanced distance of menisci based on the geometric analysis for various gaps. As the angle α increases 0° to 180°, meniscus at the widest gap advances but other menisci at narrower gaps advance until $\alpha < 90°$ and then they retreat after $\alpha > 90°$. E,F) Simulation and experimental results of meniscus dynamics. Both simulation and experimental results show two distinct phases of meniscus behavior and confirmed the analysis obtained with geometrical analysis.

2.2. Liquid Patterning Using Designed Post Arrays

Different behaviors of menisci that straddle posts of different gaps can be exploited to trap liquid within a designated region defined by densely spaced posts. **Figure 2**A shows the corresponding liquid trapping process. A microchannel of 100 μm height initially filled with water is dried through side areas that are open to the atmosphere. The microposts are arranged in different groups so that three groups of four posts that are separated by 100 μm from each other. The distance between the rectangles is 500 μm. The first image shows the picture when the dewetting front meets the posts. The menisci pass through the widest gaps in the second image as explained earlier. Eventually, liquid is trapped around the group of four posts to result in three patterned microliquid islands, as shown in the third image. Because the gap between the posts are 100 μm, the trapped volume is ≈1 nL. Figure 2B shows a series of photographs that show the dynamics of the menisci that spontaneous connect together as the meniscus from opposite sides of the microposts bulge and grow. The thin liquid film between the bulging interfaces is squeezed out of the gap, leading to the snapping of the capillary bridge. This experimental result shows same tendency and agree well with the simulation result in Figure 2C. Thus, when bulging interfaces connect with each other, array of nanoliter scale microliquid patterns can be generated inside the microchannels as shown in next figure.

2.3. CGP by Draining a Microchannel

Based on meniscus dynamics via designed microposts arrays, new method for rapid liquid patterning on microfluidic platform using simple aspiration is demonstrated. **Figure 3** shows the device design, process steps, and examples of microliquid patterns formed by CGP. To generate microliquid patterns,

www.MaterialsViews.com

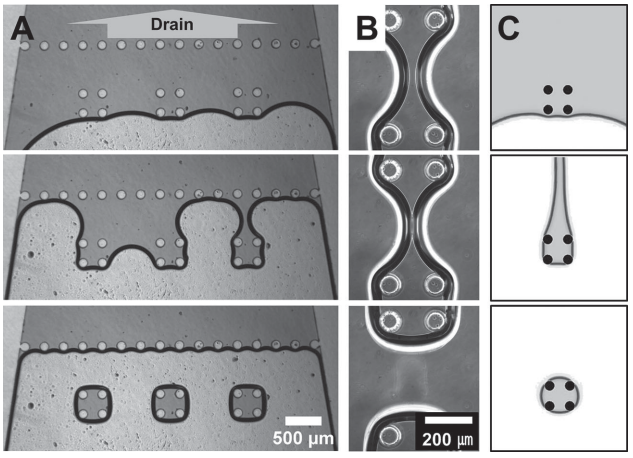

Figure 2. Microliquid patterning inside microchannels. A) Groups of closely spaced posts (100 μm apart) are arrayed (500 μm apart) across the channel width (2 mm) to trap the liquid during draining. Series of photographs show advancing menisci that move around and merge, trapping 1 nL volume of microliquid between the four posts. B) Series of magnified images of the region where two menisci opposite the closely spaced posts merge. The liquid capillary between two menisci eventually breaks when the two menisci touch and snap together. C) Simulation results showing the process of capillarity guided trapping of liquid between the posts.

liquid is first introduced into the microchannel containing the microposts array. After filling, the liquid is aspirated with bench top vacuum pump or other methods. The CGP is very robust and a variety of methods, from simple air drying to syringe pump was used to drain the channels. The CGP resulted in reproducible results over the entire microchannel. Fast removal of liquid by suction yielded identical result as the slow evaporation method. The resulting patterns were independent of the drain method and can be operated with any available equipment.

Figure 3B shows different examples of microliquid patterns, from simple array of nanoliter scale microliquid patterns to complex patterns that fill different size patterns. The photographs show patterned nanoliter size microliquid (colored dye was added for visualization). The microfluidic channels were assembled from polydimethylsiloxane (PDMS) embossed channels plasma bonded to glass coverslip. The smallest post gap distance used in these examples were 100 μm and the channel height was fixed at 100 μm. Although, smaller dimensions for channel height and gaps can be fabricated and hence result in smaller microliquid pattern, due to ease of master mold fabrication and compatibility with extended cell culture (shown later), the minimum size was fixed at 100 μm for both the gap and channel height.

In addition to the feature size of post–post distance, an important parameter of the CGP is that for hydrophilic liquid or gel, the channel surface has to be hydrophilic while for hydrophobic liquid, corresponding material surface should be hydrophobic. There is no constraint to the type of materials for the microfluidic device (PDMS, glass or others) or gel (i.e., matrigel or other ECM) or liquid (deionized water) that can be patterned provided they have similar wettability characteristics.

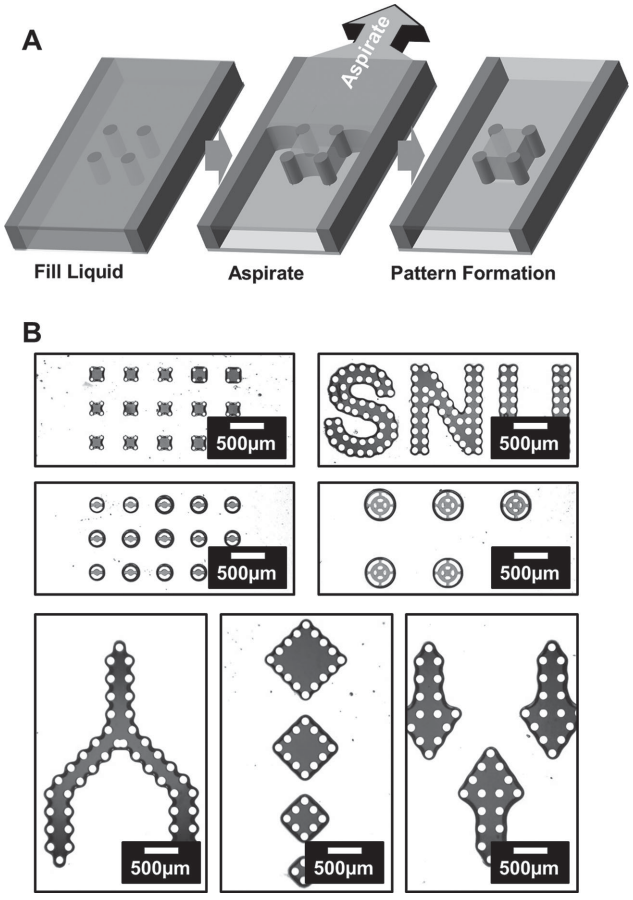

Figure 3. CGP of microliquid. A) Schematic showing the steps of CGP. A liquid filled microchannel is aspirated from one side to leave behind microliquids trapped between densely spaced posts. Simple, one-step patterning results in reproducible microliquid patterning over large areas. B) Various nanoliter scale liquid patterns formed inside microchannel by CGP. Microliquids are trapped between densely spaced posts or structures with circular posts with small openings. Placing closely spaced structures around the boundary can produce larger patterns.

After assembling the microfluidic device (surface is hydrophilic from plasma exposure), the microchannel was first filled with water. To drain the channel, a bench top vacuum pump (Δp = 4.4 kPa) was used to aspirate the liquid for ≈5 s. Because the pattern of trapped liquid is driven by surface tension of the moving liquid/air interface as the liquid is drained, the shape of post is not important. Various shapes can be used to generate complex features with varying sizes as long as the minimum gap between the posts is maintained. An entire device with 50 mm^2 or larger can be patterned by a single aspiration step that last only 5 s.

As the Figure 3B, liquid patterns produced by CGP have irregularities in shape and size. It is caused by dirt inside microchannel and spatial pressure variation. To produce uniform liquid patterns, microchannel should be clean and the opening of microstructures (gap between microstructures) should be small and perpendicular to the flow direction (like the third image of Figure 3B).

small NANO MICRO

2.4. Maximum Gap Limitations of CGP

CGP can produce microliquid patterns using a simple protocol. Unlike conventional methods where smaller patterns are more difficult to generate, the principle for CGP limits patterning of large structures (i.e., maximum gap between posts or structures). CGP is based on pinning the meniscus using predefined microstructures. To apply CGP, surface tension should the dominant force compared to inertia and gravity. In most experimental conditions, effect of gravity is negligible. Since meniscus pinning is dependent on surface tension, if inertial force is more dominant than surface tension (i.e., fast flow) meniscus cannot be reliably pinned.

To find the upper and lower limit of patterns that can be produced by CGP, we analyzed the Weber number (We), a fluid mechanical dimensionless number that provides relative importance between inertia and surface tension. When the Weber number equals to 1, inertial force and surface tension are equally operative, but when it is smaller than 1, surface tension is more dominant. To apply CGP inside microfluidic channels, Weber number should be smaller than 1 (i.e., $We = \rho u^2 L/\sigma << 1$, ρ: density of fluid, u: velocity, L: post gap, σ: surface tension). Substituting the values used for the experimental conditions ($\rho = 1000$ kg m^{-3}, $\sigma = 0.07$ N m^{-1}, and $u = 0.55$ m s^{-1}), the maximum gap (when We = 1) between posts was L = 231.4 μm. Here the characteristic liquid velocity u corresponds to the average flow velocity in a microchannel for a pressure drop of 4.4 kPa along the channel length of 2 cm.

Figure 4A shows the theoretical limit of maximum gap size as a function of pressure difference (ΔP) for various channel height (50–200 μm). As expected, when inertial force is increased by using larger ΔP, maximum gap that can be used to trap microliquids using CGP decreases as well. When microchannel height is increased from 50 to 200 μm, the maximum gap size decreases dramatically from ≈3000 to 15 μm. As indicated on the figure, for 100 μm high microchannels, the maximum calculated gap size is 231.4 for ΔP (4.4 kPa used in actual experiments). The experimental verification using 100 μm high microchannel is shown in Figure 4B. A series of patterns with gaps between 100 and 500 μm were fabricated and tested. As predicted from theoretical calculations in Figure 4A, gaps up to 200 μm are successfully and reliably trapped by CGP. However, for patterns starting at 250 μm and above, the trapping is inconsistent and random. As discussed earlier, the maximum gap limit can be affected by properties of liquid (i.e., density, viscosity, and surface tension), microchannel dimensions (i.e., length, width, and height) and applied vacuum pressure. Thus when used with precise pressure controller, various complex patterns of various sizes can be patterned using CGP.

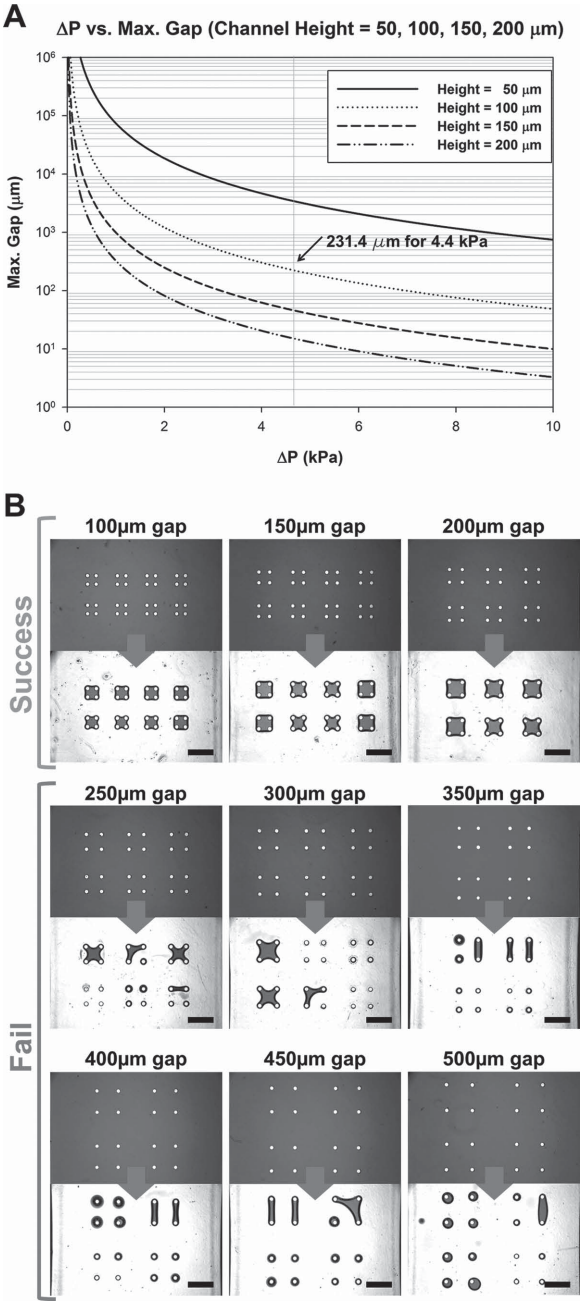

Figure 4. Limitation of CGP 1: Maximum gap. A) Theoretical analysis of the maximum gap limit of CGP according to the pressure differences (ΔP) and channel heights. The gap limits were calculated using the Weber number which stands for the relative importance between inertia and surface tension. As a result, theoretical limit of CGP was 231.4 μm with the conditions used in this experiment (channel height = 100 μm, ΔP = 4.4 kPa). B) Experimental results to find gap limit of CGP. Microliquids were successfully patterned when the gaps between two microposts were 200 μm or shorter. However, consistent with the theoretical analysis, microliquids were not patterned when the gaps were larger than 200 μm. Scale bar = 500 μm.

2.5. Patterning of Multiple Nested Materials by Sequential CGP

Using the new CGP method, complex patterns with different materials can be patterned that are difficult to obtain with conventional photolithography or soft lithography techniques. Multiple nested materials (i.e., Russian doll-like pattern) or isolated array of small micropatterns can be readily formed as shown in **Figure 5**. In this experiment, we used photo-curable hydrogel (PEG-DA) to visualize the shape and colors of patterns. Figure 5A shows the schematic of the fabrication

www.MaterialsViews.com

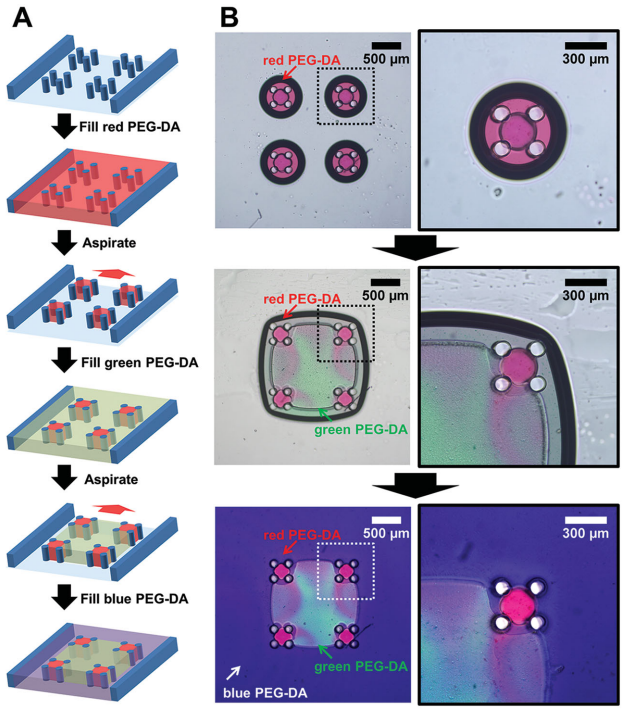

Figure 5. Nested patterning of multiple materials by sequential CGP. A) Repeated filling and aspiration result in patterning of multiple materials. First, the channel is filled with first liquid. Perform first CGP to pattern microliquids inside densely placed post arrays (groups of four posts in the schematic). Solidify the first material (red PEG-DA) by UV exposure. These patterns act as "new posts." Repeat second CGP to trap and solidify second material (green PEG-DA). Third material, blue-PEG-DA is filled into the rest of the channel and solidified. In this manner, multiple nested patterns can be obtained. B) Experimental results of multiple nested patterns. Three kinds PEG-DA (mixed with red, green, and blue ink for visualization) were successfully patterned.

process for patterning three different types of photo-curable hydrogels. To demonstrate the potential, we used a simple design that contained an array of posts to trap red, green, and blue labeled PEG-DA (UV curable polymer mixed with color ink). The post arrays are made up of groups of four posts (d = 100 μm, gap = 100 μm) that are placed in periodic array with distance of 500 μm from other groups. The width of the channel was 2 mm. Repeated steps of filling, aspiration, UV exposure are repeated to generate the patterns. For the first pattern-trapped by the group of four smallest posts, the channel was filled with red PEG-DA and aspirated to generate an array of ≈1 nL patterns. These first patterns were used subsequently to trap the second material (green PEG-DA) with larger size features, ≈25 nL. Finally, blue PEG-DA was filled into the entire channel and solidified to encapsulate the array of two different materials. Using the patterns generated from previous steps, multiple hierarchical structures can be patterned using this method (Figure 5B). As shown in following sections, cell containing 3D gels can be patterned into arbitrary configuration for different biological investigations such as coculture of cancer and HUVECs as shown in Figure 7.

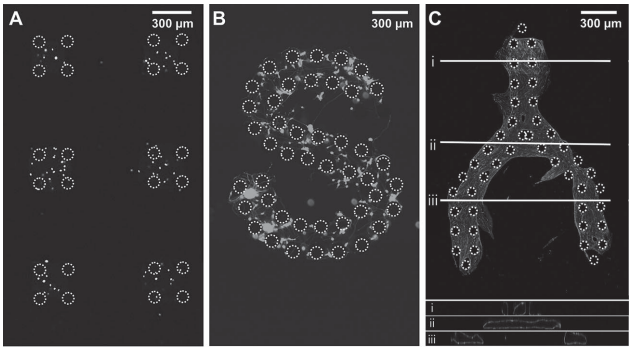

Figure 6. Applications of CGP for biology: patterning cells. A) Isolated array of cell patterns was obtained using CGP. Microalgae, *C. reinhardtii,* in alginate gel (chlorophyll autofluorescence) was trapped between posts over large area. The array of cells can be used to optimize conditions for biodiesel production. B) Designed neural network formed with primary rat cortical neurons (Calcein AM-labeled) in 3D matrigel. The neurons are healthy and show several neuritis and axons. C) Engineered blood vessel with branched Y-shape. HUVECs (CD31-labeled) were mixed with fibrin gel and patterned inside designed post array.

2.6. Patterning Cells in 3D ECM

We envision that the CGP will find many applications in development of biological assay systems where cells need to be patterned in an array of single cells or coculture conditions. **Figure 6** shows various examples that demonstrate proof of concept cellular patterns for high-throughput long-term monitoring of *Chlamydomonas reinhardtii* (Figure 6A), formation of neuronal networks (Figure 6B), and formation of predefined shape of blood vessel networks (Figure 6C).

C. reinhardtii is model green alga that is widely studied for potential applications in sustainable biofuel research and CO_2 mitigation. Algae are usually cultured in large scale and single cell-level investigation has not been performed widely. Microfluidics is a platform where precise culture conditions (i.e., nutrient, carbon source, pH, etc.) can be controlled precisely.

In Figure 6A, an array of immobilized *C. reinhardtii* (≈1 nL trapped volume) within alginate hydrogel is shown. Chlorophyll autofluorescence allowed imaging without additional staining. Single cells as well as groups of cells can be trapped reliably. The picture was taken after 1 day of culture. The formation of *C. reinhardtii* array was obtained in simple two steps similar to examples shown earlier. The liquid was replaced with *C. reinhardtii* was mixed with alginic acid and patterned by CGP. After trapping the cell containing alginic acid, calcium containing media was filled into the channel to cross-link the hydrogel. We have successfully cultured the cells for 7 days and observed proliferation inside the alginate gel. An advantage of such array of immobilized *C. Reinhardtii* is that culture conditions can be varied dynamically or a combinatorial mixture of various nutrients can be exposed to the array and the cellular response can be observed in real-time using optical microscopy.

Figure 6B shows a photograph of neural network formed with primary rat cortical neurons. The neurons were captured in 3D matrigel matrix of artificial shape and the

small NANO MICRO

pattern was 2 mm long with post–post spacings of 100 μm. Primary neurons were suspended in media and equal volume of liquid matrigel was mixed immediately before filling the device. After gentle aspiration to pattern the gel, entire device was placed in an incubator to allow gelation of matrigel. Media was added after 3 min. and the culture was maintained following usual protocol. This result demonstrates that the neurons are viable (photograph was taken after 7 days in vitro, calcein acetoxymethyl (AM) viability stain) and show healthy neuritic processes. Exposure to shear stress during CGP process was not detrimental to neurons, one of the most sensitive cells to shear and culture conditions, and that the patterning process is compatible with mammalian cells.

The fluorescent image in Figure 6C shows a 2 mm long Y-shaped network of blood vessel. The microchannel was first filled with HUVEC suspension in fibrinogen–thrombin mixture (liquid state, before cross-linking). Before fibrin clotted (≈1 min), it was gently aspirated to leave the trapped gels behind. After cross-linking for 1 min at room temperature, the channel was filled with lung fibroblast (LF) and media. The HUVEC–LF coculture was maintained for 5 days to allow blood vessel network formation.

The photograph shows HUVECs stained with CD31, a marker of endothelial cells (LFs were not stained for clarity). Confocal cross-section images at three positions along the pattern clearly show lumens formed by the HUVECs. This result illustrate that when HUVECs are patterned into arbitrary shaped gel, perfusable network can be formed that are guided by the design.

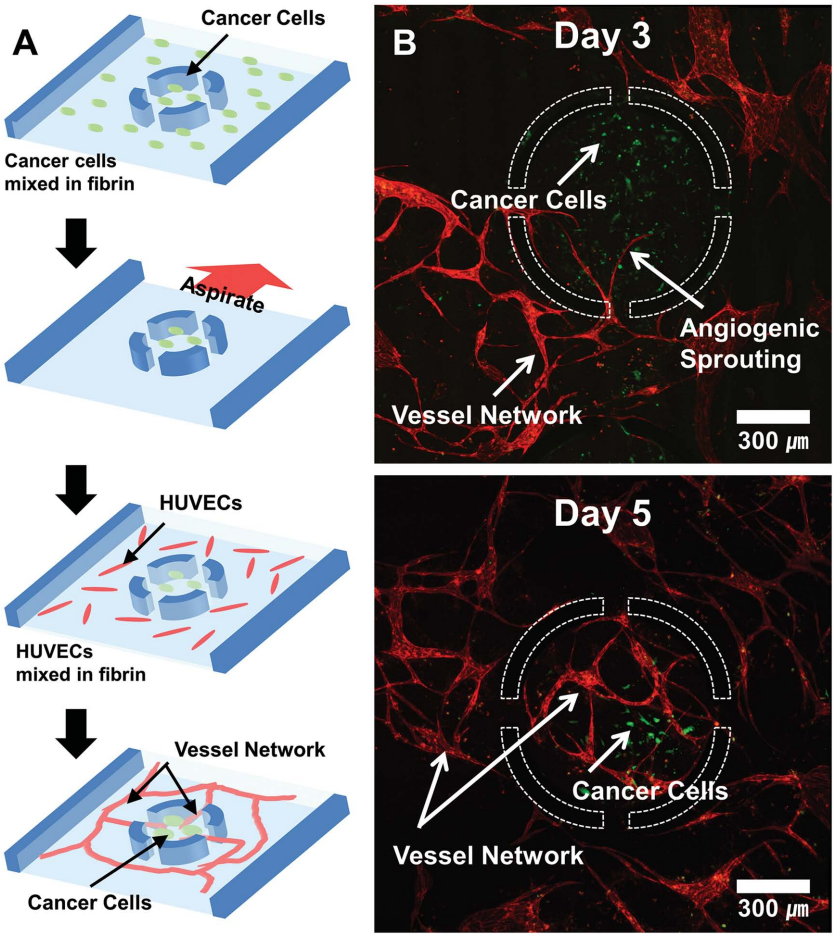

Figure 7. In vitro model of cancer angiogenesis. Cancer cells (U87MG) and HUVECs were patterned in close proximity. This coculture model was established in three simple steps. Cancer cells were first trapped within circular areas by CGP and the rest of the channel was filled with HUVEC and LF mixture in fibrin matrix. A) HUVECs have formed vessel networks and some vessels have started entering the area densely populated with cancer cells 3 days after plating the cells. B) By day 5, numerous vessels have entered the circular cancer cell area, attracted by U87MG. The vessels have lumens and are visualized with CD31 (EC marker).

2.7. Cancer Angiogenesis Model by Sequential CGP

Cancer cell migration and angiogenesis is a 3D process that involves cell–cell and cell–ECM interactions that are difficult to recapitulate in 2D culture platforms. Recently, several models have been developed to study these processes in 3D gels. However, none of these models can approach the simplicity of 2D experiments using a petri dish. We aimed to develop a new in vitro model of angiogenesis that is simple and robust. Angiogenesis is a process of sprouting new blood vessel stimulated by paracrine signals from nearby cancer cells. We have patterned cancer cells and HUVECs in close proximity (less than 100 μm apart for paracrine signaling to be effective) and observed the angiogenesis toward the tumor cells.

Figure 7A shows the cell loading and patterning steps for cancer angiogenesis model. We have used a circular trap with four openings (opening size = 100 μm) to localize cancer cells (U87MG, highly angiogenic glioblastoma cells) and surrounded them with HUVECs and LFs. The channel is 100 μm high, producing 3D environment for the cells. Similar to group of four posts shown earlier, the circular traps are as effective in capturing U87MG cells. The shape of the structures can be designed for each application to trap different amounts/number of cells. In this case, we wished to observe the angiogenic process with time-lapse microscopy and the well-defined arrayed patterns allowed continuous imaging of a number of areas on a single chip.

Figure 7B shows fluorescence images of area around the patterned circular trap filled with cancer cells (green fluorescent protein (GFP) labeled U87MG) in fibrin. The HUVECs, placed outside the trap spontaneously form network of blood vessels after 3 days. They are clearly visible (red, CD31 stain) around the traps. By day 3, HUVEC sprouts begin to enter the circular trap area that was filled with U87MG,

a glioblastoma cell line that is highly angiogenic. By day 5, somewhat dense network of vessels are visible inside the circular region as the blood vessels have penetrated the area occupied by the cancer cells. The presence of U87MG cells clearly influenced and directed sprouting angiogenesis toward themselves. These blood vessels have open lumen like the example shown in Figure 7C.

In a simple three-step process, a 3D cancer angiogenesis model that mimics cell–cell and cell–ECM interactions has been engineered in a microfluidic device. This model can be further developed to recapitulate the structure and organization of tumor microenvironment that is amenable to long-term observation of dynamic events such as angiogenesis and cancer cell migration during metastasis.

3. Conclusion

We developed a simple nonlithographic patterning method by engineering meniscus dynamics when a liquid filled channel is drained. When microstructures are strategically placed, surface tension-driven trapping of liquids take place as advancing menisci snap and merge, spontaneously generating isolated microliquids. Detailed analysis of the meniscus dynamics based on hydrodynamics resulted in understanding the factors that influence meniscus advancement during channel draining. We formulated meniscus dynamics between microstructures as a function of α (angle between the center of post and the contact point of meniscus at the largest gap) and gap distance and determined conditions where adjacent advancing menisci snap and merge around structures to trap microliquids. Based on this geometric analysis, arbitrary isolated microliquid and gel patterns were generated by strategically placed microstructures. The CGP process is extremely robust, yielding reproducible patterns under variable experimental conditions. Nanoliter scale liquids or gels containing single cells can be reliably patterned over large areas. The patterning process is extremely simple and fast. Filling of the channel followed by draining (vacuum aspiration, natural drying, or others) instantaneously generates patterns over the entire microfluidic device. For microchannels that are hydrophilic, water or gels instantaneously fill the entire channel (even for circular traps with small openings, i.e., Figures 3B and 7). Application of vacuum aspiration at one end of the channel is all that is needed to obtain the patterns. One step of CGP takes less than 5 s to generate the patterns.

A novel patterning method based on fluid dynamics is described and also the limitations of the method are analyzed both theoretically and experimentally. CGP was used to trap single cells or groups of different cells (for coculture) to build an in vitro platform for on chip drug screening and organ-on-a-chip applications. A few improvements await to be implemented in the future to make this process more viable in actual applications. It is necessary to increase the uniformity of the post surfaces to remove the irregularity of contact line pinning process, which may result in variations in volumes of trapped liquid. A novel way to release patterned liquids during or after use might be desirable in some applications, which may require external supply of energy or materials into the system.[34] We believe that the simplicity and robustness of the method will be attractive for a number of biological experimental platforms that involve engineering 3D cell microenvironment.

4. Experimental Section

Microfluidic Device Fabrication: Microfluidic devices were fabricated using soft lithography. Master molds for soft lithography were fabricated by patterning negative tone photoresist SU8-100 (MicroChem, Newton, MA) with 100 μm thickness on Si wafers (Silicon Sense, Boise, ID) by typical photolithography. Positive replicas with embossed channels were fabricated by molding PDMS (Sylgard 184, Dow Corning, Midland, MI) against the master mold. The PDMS prepolymer was mixed with curing agent by 10:1(w/w) ratio. The PDMS poured master was placed on hot plate (95 °C) for curing PDMS. Cured PDMS was then separated and inlet and outlet reservoirs for fluidic interconnects were punched with sharpened needles. The PDMS piece was irreversibly bonded to a glass slide upon treating both with an air-plasma generator (Femto Science, South Korea), forming the microfluidic device.

Modeling of Meniscus Dynamics: A 2D simulation was performed using Matlab (MathWorks, Natick, MA) and COMSOL Multiphysics (Comsol, Palo Alto, CA) to model the dynamics of meniscus at liquid–air interface with.

Cell Culture: C. reinhardtii (CC-503) in tris acetate phosphate medium were cultured at 23 °C and 5% CO_2 while shaking on an orbital shaker at 125 rpm. The cultures were exposed to 12 h cycles of light (40 μmol s^{-1} m^{-2}) and dark.

Primary cortical neurons were extracted from embryonic Sprague-Dawley rats (TP18). Cortices were extracted and dissected in 1× Hank's balanced salt solution (HBSS). Then it was treated with 3 mL of 0.125% trypsin/ethylenediaminetetraacetic acid (EDTA) for 15 min in a 37 °C water bath. The trypsin/EDTA was removed by rinsing three times with HBSS, after which 1 mL of plating medium Dulbecco's Modified Eagle Medium (DMEM) with 10% fetal bovine solution (FBS) was added, and the mixture was centrifuged for 1 min at 1100 rpm. The supernatant was then discarded, and 2 mL of a neurobasal medium(Gibco) containing 2% of supplement B-27, 0.25% GlutaMax media supplement, and 1% Pen/Strep (Invitrogen, Carlsbad, CA) was added. The cells were triturated using a Pasteur pipette. The cell suspension was filtered through a cell strainer with a pore size of 22 μm and the cell viability and density were determined by trypan blue staining. All procedures performed were approved by the Institute of Laboratory Animal Resources (ILAR) at Seoul National University, Korea.

HUVEC (Lonza) were cultured in Endothelial Growth Medium (EGM-2, Lonza). Normal human LFs (Lonza) were cultured in Fibroblast Growth Medium-2 (Lonza). Human glioblastoma multiforme cells, U87MG (ATCC, Virginia) were cultured in DMEM supplemented with 10% FBS, penicillin (100 Units mL^{-1}) and streptomycin (100 Units mL^{-1}). All cells were cultured in a humidified incubator at 37 °C and 5% CO_2.

Cell Loading: C. reinhardtii suspension was mixed in 1:1 ratio with alginate(Sigma) solution (8%, w/v) with final concentration 5×10^6 cells mL^{-1}. It was polymerized after patterning with $CaCl_2$ (10%, w/v) as in Figure 5A.

Primary rat cortical neurons were mixed with matrigel (BD Biosciences, San Jose, CA) in 1:1 ratio with final concentration of 6×10^6 cells mL^{-1} and polymerized after aspiration. With culture media filled inside the channel, it was incubated for 5 days to form a network (Figure 5B).

To obtained designed blood vessel network as shown in Figure 5C, HUVECs were suspended in fibrinogen solution (2.5 mg mL^{-1} fibrinogen with 0.15 Units mL^{-1} of aprotinin and 0.5 Units mL^{-1} of thrombin) at a concentration of 15×10^6 cells mL^{-1} and patterned using CGP. After aspiration, the cell–fibrin mixture was placed in an incubator for 2 min for polymerization. The microchannel was loaded with EGM-2 medium with LFs at a concentration of 1.5×10^6 cells mL^{-1}. Devices were incubated for 4–5 days and media was changed every 2 days to obtain lumenized blood vessel.

For in vitro cancer angiogenesis model as shown in Figure 6, U87MGs were mixed with fibrinogen solution at a concentration of 0.6×10^6 cells mL^{-1}. Mixture was injected and quickly aspirated to trap the cancer cells inside the circular pattern. After 2 min of incubation to obtain crosslinked fibrin, HUVEC, and LF mixture with fibrinogen solution with concentration of 10×10^6 and 1×10^6 cells mL^{-1}, respectively, were injected into the channel then cured. EGM-2 media was added to the reservoirs at the each end of the channel and remained in the incubator with media change every other day.

PEG-DA Photopolymerization: To perform multiple material patterning, UV curable polymer, PEG-DA (MW: 258, mixed with 3%DMPA for photo initiator) mixed with color ink was used. PEG-DA was cross-linked with a UV lamp (22 mW cm^{-2}) for 15 s.

Immunostaining: To image *C. reinhardtii*, autofluorescence signal from chlorophyll was used. Primary rat cortical neurons were stained with Calcein AM (Molecular Probes). For imaging endothelial cells, mouse monoclonal antibody specific for human CD31 (AlexaFluor1647, clone WM59, BioLegends) were used and Hoechst 33342 (Molecular Probes) was used to stain the nuclei. CellTracker Green CMFDA (5-chloromethylfluorescein diacetate, Molecular Probes) was used to stain U87MG cancer cells. All cells were stained before loading.

Imaging: Olympus FV1000 confocal microscope was used for 3D cross-sectional imaging. Images were analyzed with imageJ and IMARIS (Bitplane, Switzerland).

Acknowledgments

This work was supported by National Research Foundation of Korea (Grant Nos. NRF-2014M1A8A1049278 and 2014023206), funded by the Ministry of Science, ICT and Future Planning via SNU IAMD.

[1] Y. Xia, G. M. Whitesides, *Annu. Rev. Mater. Sci.* **1998**, *28*, 153.
[2] D. C. Duffy, J. C. McDonald, O. J. Schueller, G. M. Whitesides, *Anal. Chem.* **1998**, *70*, 4974.
[3] G. M. Whitesides, E. Ostuni, S. Takayama, X. Jiang, D. E. Ingber, *Annu. Rev. Biomed. Eng.* **2001**, *3*, 335.
[4] A. M. Taylor, M. Blurton-Jones, S. W. Rhee, D. H. Cribbs, C. W. Cotman, N. L. Jeon, *Nat. Methods* **2005**, *2*, 599.
[5] D. Di Carlo, N. Aghdam, L. P. Lee, *Anal. Chem.* **2006**, *78*, 4925.
[6] D. Di Carlo, L. Y. Wu, L. P. Lee, *Lab Chip* **2006**, *6*, 1445.
[7] S. Lindström, H. Andersson-Svahn, *Lab Chip* **2010**, *10*, 3363.
[8] K. Osada, M. Hosokawa, T. Yoshino, T. Tanaka, *Analyst* **2014**, *139*, 425.
[9] H. Andersson, A. van den Berg, *Sens. Actuators B* **2003**, *92*, 315.
[10] S. W. Rhee, A. M. Taylor, C. H. Tu, D. H. Cribbs, C. W. Cotman, N. L. Jeon, *Lab Chip* **2005**, *5*, 102.
[11] M. S. Hahn, J. S. Miller, J. L. West, *Adv. Mater.* **2006**, *18*, 2679.
[12] H. Lee, S. Kim, M. Chung, J. H. Kim, N. L. Jeon, *Microvasc. Res.* **2014**, *91*, 90.
[13] H. Lee, M. Chung, N. L. Jeon, *MRS Bull.* **2014**, *39*, 51.
[14] A. Hasan, A. Memic, N. Annabi, M. Hossain, A. Paul, M. R. Dokmeci, F. Dehghani, A. Khademhosseini, *Acta Biomater.* **2014**, *10*, 11.
[15] J. Hong, J. B. Edel, A. J. de Mello, *Drug Discovery Today* **2009**, *14*, 134.
[16] D. Wlodkowic, S. Faley, M. Zagnoni, J. P. Wikswo, J. M. Cooper, *Anal. Chem.* **2009**, *81*, 5517.
[17] D. Huh, B. D. Matthews, A. Mammoto, M. Montoya-Zavala, H. Y. Hsin, D. E. Ingber, *Science* **2010**, *328*, 1662.
[18] D. Huh, Y. S. Torisawa, G. A. Hamilton, H. J. Kim, D. E. Ingber, *Lab Chip* **2012**, *12*, 2156.
[19] J. L. Wilbur, A. Kumar, H. A. Biebuyck, E. Kim, G. M. Whitesides, *Nanotechnology* **1996**, *7*, 452.
[20] D. Qin, Y. Xia, G. M. Whitesides, *Nat. Protoc.* **2010**, 491.
[21] D. Bodas, C. Khan-Malek, *Sens. Actuators B* **2007**, *123*, 368.
[22] V. N. Truskett, M. P. Watts, *Trends Biotechnol.* **2006**, *24*, 312.
[23] C. P. Huang, J. Lu, H. Seon, A. P. Lee, L. A. Flanagan, H.-Y. Kim, A. J. Putnam, N. L. Jeon, *Lab Chip* **2009**, *9*, 1740.
[24] Y. Shin, S. Han, J. S. Jeon, K. Yamamoto, I. K. Zervantonakis, R. Sudo, R. D. Kamm, S. Chung, *Nat. Protocols* **2012**, *7*, 1247.
[25] S. E. Chung, W. Park, S. Shin, S. A. Lee, S. Kwon, *Nat. Mater.* **2008**, *7*, 581.
[26] M. S. Hahn, L. J. Taite, J. J. Moon, M. C. Rowland, K. A. Ruffino, J. L. West, *Biomaterials* **2006**, *27*, 2519.
[27] B. El Debs, R. Utharala, I. V. Balyasnikova, A. D. Griffiths, C. A. Merten, *Proc. Natl. Acad. Sci. USA* **2012**, *109*, 11570.
[28] X. T. Zheng, L. Yu, P. Li, H. Dong, Y. Wang, Y. Liu, C. M. Li, *Adv. Drug Delivery Rev.* **2013**, *65*, 1556.
[29] W. Gu, X. Zhu, N. Futai, B. S. Cho, S. Takayama, *Proc. Natl. Acad. Sci. USA* **2004**, *101*, 15861.
[30] Y.-C. Tung, Y. S. Torisawa, N. Futai, S. Takayama, *Lab Chip* **2007**, *7*, 1497.
[31] D. R. Gossett, W. M. Weaver, N. S. Ahmed, D. Di Carlo, *Ann. Biomed. Eng.* **2011**, *39*, 1328.
[32] M. C. Park, J. Y. Hur, K. W. Kwon, S.-H. Park, K. Y. Suh, *Lab Chip* **2006**, *6*, 988.
[33] B. P. Casavant, E. Berthier, A. B. Theberge, J. Berthier, S. I. Montanez-Sauri, L. L. Bischel, K. Brakke, C. J. Hedman, W. Bushman, N. P. Keller, *Proc. Natl. Acad. Sci. USA* **2013**, *110*, 10111.
[34] X. Huang, W. Hui, C. Hao, W. Yue, M. Yang, Y. Cui, Z. Wang, *Small* **2014**, *10*, 758.

Received: December 3, 2014
Revised: January 9, 2015
Published online: February 10, 2015

